

Maser maps and magnetic field of OH 300.969+1.147

J. L. Caswell¹, B. Hutawarakorn Kramer^{2,3}, and J. E. Reynolds¹

¹ *Australia Telescope National Facility, CSIRO, PO Box 76, Epping, NSW 2121, Australia; james.caswell@csiro.au*

² *Max-Planck-Institut für Radioastronomie, Auf dem Hügel 69, 53121 Bonn, Germany; bkramer@mpifr-bonn.mpg.de*

³ *National Astronomical Research Institute of Thailand, Physics Building, Chiang Mai University, Chiang Mai 50200, Thailand; busaba@narit.or.th*

Accepted . Received ; in original form 2009

ABSTRACT

The southern maser site OH 300.969+1.147 has been studied using the Long Baseline Array of the Australia Telescope National Facility. The 1665- and 1667-MHz hydroxyl ground-state transitions were observed simultaneously. A series of maps with tenth-arcsec spatial resolution, at velocity spacing 0.09 km s^{-1} , and in both senses of circular polarization, reveal 59 small diameter maser spots. The spots are scattered over 2-arcsec, coincident with a strong ultracompact H II region, at a distance of 4.3 kpc. 17 Zeeman pairs of oppositely polarized spots were found, all yielding magnetic field estimates towards us (negative), ranging from -1.1 to -4.7 mG, with a median value of -3.5 mG. Excited state masers of OH at 6035 MHz and 6030 MHz at this site also display Zeeman pairs revealing a magnetic field of -5.0 mG. Weak methanol maser emission is intermingled with the OH masers, but there is no detectable closely related water maser. The consistent magnetic field direction found within this site is a striking feature of several other maser sites associated with strong H II regions studied in comparable detail. We interpret the site as a mature region nearing the end of the brief evolutionary stage that can support maser emission.

Key words: masers - stars: formation - H II regions - ISM: molecules - radio lines: ISM.

1 INTRODUCTION

Molecular maser emission associated with newly formed massive stars commonly comprises many small spots spread over a site of typical extent 30 milliparsec, enveloping the star. Hydroxyl masers are especially useful probes of the immediate surroundings of the star since the Zeeman effect leads to a readily measurable separation of left and right circularly polarized emission in magnetic fields of a few mG. At most maser sites, it requires the high spatial resolution of Very Long Baseline Interferometry to unequivocally recognise individual Zeeman patterns, and to explore the homogeneity of the magnetic field within the masing region. Pioneer observations began more than two decades ago, and there has now been increased recent activity from the VLBA, with new results for 18 targets (Fish, Reid, Argon & Zheng 2005). The target properties are found to be diverse, but hint at clearly recognisable classes of object, demonstrating a need for similar studies of the numerous potential targets in the southern hemisphere.

The southern hemisphere Long Baseline Array (LBA) of the Australia Telescope National Facility (ATNF) allows high frequency resolution over a total bandwidth spanning both the 1665- and the 1667-MHz ground-state OH transi-

tions. Using three stations, the spatial resolution of approximately 100 milliarcsec (mas) is quite well suited to observations of masers at distances of a few kpc; it allows clear position discrimination between the numerous tight clusters of spots (of typical size $< 100 \text{ mas}$) that are commonly spread over a total extent of an arcsec.

Our program with the LBA to study the rich variety of masers in the southern sky began with OH 323.459-0.079 (Caswell & Reynolds 2001); the present study is similar, but improved by a lower noise level, and analysed at higher spectral resolution.

2 OBSERVATIONS

Observations were made over a 15h period 2000 August 17. The array comprises the Parkes 64-m antenna, complemented by a 22-m paraboloid at Mopra, and the compact array of the Australia Telescope (ATCA) at Narrabri operating as a tied array (equivalent in sensitivity to a dish of 46-m diameter). These yield baselines of approximately 119 km, 203 km and 321 km, predominantly north-south. The S2 tape system recorded both right- and left-hand senses of

circular polarization (RHCP, LHCP) simultaneously, with a bandpass centred at 1667 MHz, and limited to a 4-MHz bandwidth by a digital filter with excellent flat response in amplitude and phase. Our strategy was to observe a target for 25-min periods, bracketed by 5-min periods on a phase and secondary amplitude calibrator (1148-671, 1215-457 or 1740-517, with total intensity flux densities of 1.78, 3.37 and 7.47 Jy). Flux densities are relative to the absolute calibration derived from 1934-638 (unpolarized, with total intensity of 14.157 Jy). The target position of 300.969+1.147 (J2000 RA $12^{\text{h}}34^{\text{m}}53.20^{\text{s}}$, Dec. $-61^{\circ}39'40.0''$) was alternated with another target (337.505-0.053, to be discussed in a later paper) for the period when both were accessible to the Parkes telescope.

3 DATA REDUCTION

Each baseline required a unique correlator pass in order to achieve the high frequency resolution of 8192 channels across the 4-MHz band. The output from correlation of the signals from each polarization was binned into 5-sec integration periods. In the subsequent processing using the AIPS reduction package, no Hanning smoothing was applied so that the final channel separation remains 0.48828125 kHz ($= 0.088$ km s^{-1}), and the final velocity spectral resolution is 0.105 km s^{-1} (larger than the channel separation by a factor of 1.2 for uniform weighting).

The calibrators were used to derive first order phase and amplitude corrections to the target source observations, and this calibration also established the correct phase between RHCP and LHCP (and subsequently ensures precise registration of their relative positions). The program ‘cvel’ was used to align channels to the same velocity, and allow for the varying Doppler correction arising from the Earth’s motion during the observations, adopting rest frequency values of 1665.4018 and 1667.359 MHz. After perusal of spectra from each polarization, strong channels were selected, from which preliminary maps were made.

Maps of the field using only the preliminary calibration did not allow the measurement of an absolute position. However the strongest (15-Jy) spectral feature, RHCP 1665 MHz at velocity -39.8 km s^{-1} , has a known position derived from ATCA observations (Caswell 1998) of RA $12^{\text{h}}34^{\text{m}}53.24^{\text{s}}$, Dec. $-61^{\circ}39'40.3''$, with an uncertainty of 0.4 arcsec. It would be possible to use this feature as a phase reference to determine positions of all other features. However, it turns out that a RHCP 1667-MHz feature of somewhat lower amplitude, at velocity -35.8 km s^{-1} , is more suitable as a phase reference since it is more clearly distinct from other spectral features. Relative to the ATCA measured feature, we show later from the current LBA observations that it is located at larger RA by 0.03s ($= 0.22$ arcsec) and north by $0.67''$, ie at RA $12^{\text{h}}34^{\text{m}}53.27^{\text{s}}$, Dec. $-61^{\circ}39'39.63''$. This RHC 1667-MHz feature was then used as the reference feature for the maps. The uncertainty in this absolute registration remains the same as the ATCA measurement, approximately 0.4 arcsec.

This final calibration of all data relative to a single RHCP 1667-MHz feature reduces phase errors, establishes a correct absolute position, and maintains correct relative positions between polarizations and between transitions.

In the velocity range -44 to -33 km s^{-1} , ‘cleaned’ maps

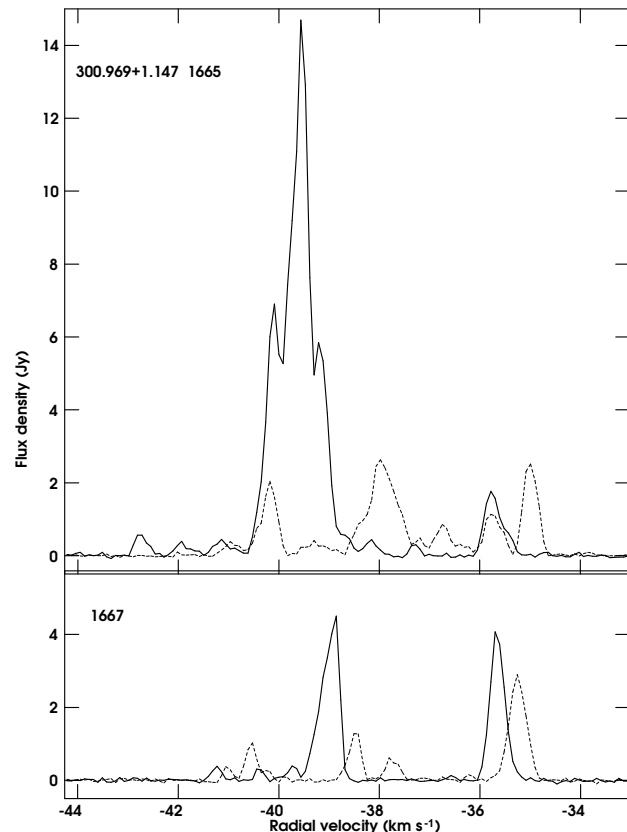


Figure 1. Spectra of the 1665- and 1667-MHz OH transitions towards OH 300.969+1.147, taken 2000 Aug 17. The two circular polarizations are distinguished as RHCP (thick line) and LHCP (thin broken line). The intensities are scaled such that the total flux density is the sum (not the average) of the two circular polarizations. The spectra comprise emission from many individual spots distributed over approximately 2 arcsec, as revealed by the LBA maps.

were made of each spectral line channel (total 128 channels) for both transitions, and for both circular polarizations. The cellsize used was 25 mas, and the restoring beamwidth was 72×130 mas (major axis at position angle 94°). The typical rms noise on a map was 8 mJy, allowing reliable detections of features down to 50 mJy, or weaker if present over several channels. At the few velocities where a strong feature exceeding 2 Jy is present, the detection of weak features at some positions is limited by dynamic range (owing to occasional 5 per cent sidelobe levels).

4 RESULTS

4.1 OH Spectra, maser spot positions and morphology

OH spectra in Fig. 1 show the total maser emission from the site at 1665 and 1667 MHz using the present observations. Earlier spectra, recorded 1982 February, can be seen in Caswell & Haynes (1987a), and are similar to those measured when it was discovered (Robinson et al. 1974). The

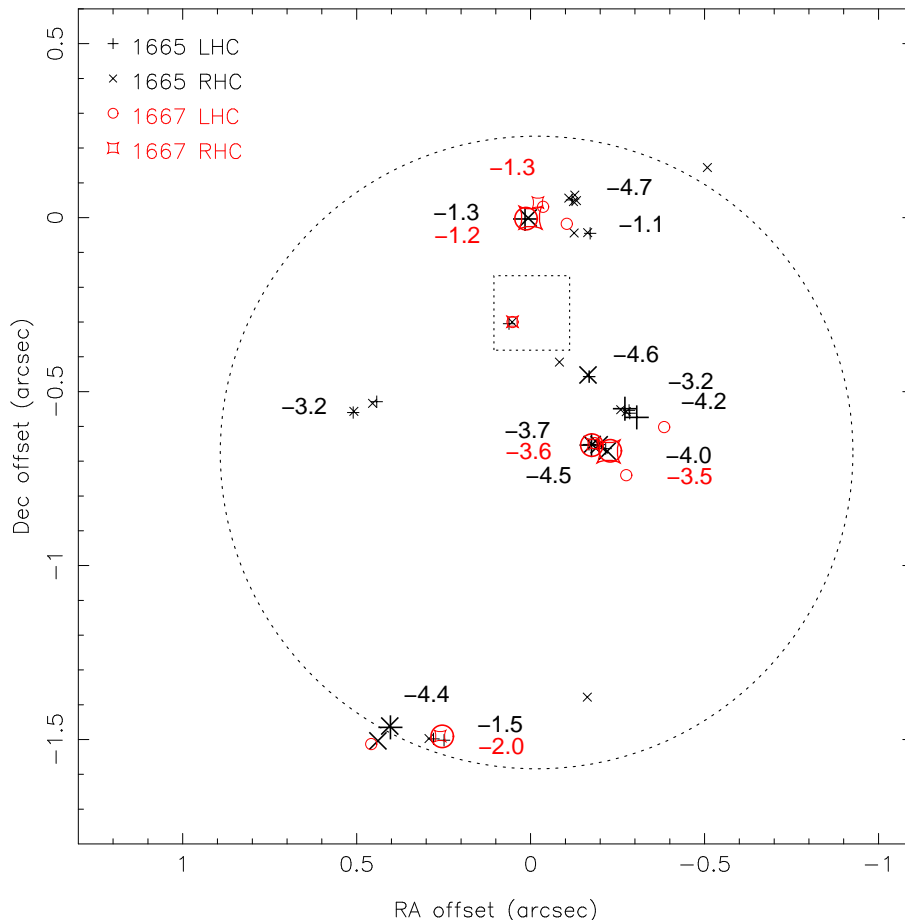


Figure 2. Spatial distribution of 59 maser spots in OH 300.969+1.147, with map reference position at RA $12^h 34^m 53.27^s$, Dec. $-61^\circ 39' 39.63''$. The distributions of RHCP and LHCP for both the 1665 and 1667-MHz transitions are superposed and denoted by different-shaped symbols. Larger symbols denote features with peaks of 0.5 Jy or greater. The Zeeman pairs are identified by the magnetic field value (mG) labelled near the corresponding pair. The field derived at 1665 MHz is shown above the value derived at 1667 MHz when Zeeman pairs at the two transitions essentially coincide. See Table 1 for precise parameters of spectral features. The approximate location of associated maser emission at 6035 MHz is denoted by a small dotted square. The approximate boundary of an underlying H II region is shown as a large dotted circle.

present spectra from 2000 August (Fig. 1) resemble the earlier spectra, but have higher sensitivity. Subsequent spectra from the Parkes telescope in 2004 November and 2005 October again resemble earlier spectra. Measurements of weak linear polarization in these new spectra will be discussed later insofar as they assist interpretation of the LBA maps which were not analysed for linear polarization.

From the ‘cubes’ of the images of RHCP and LHCP at 1665 and 1667 MHz, all emission features were measured using the ‘imfit’ task in AIPS to derive positions and flux densities, and all appear to be of small angular size (< 25 mas) relative to the beamwidth of 72×130 mas.

The positions measured for 59 individual features, corresponding to maser ‘spots’, are listed in Table 1; they are spread over an elliptical region elongated 1.66 arcsec north-south. Each row of Table 1 lists a narrow spectral feature (typically 0.4 km s^{-1} to halfpower), in a single sense of circular polarization, at one of the two OH transitions of 1665 or 1667 MHz. The maser features are grouped by transition and sense of circular polarization, and then ordered by radial velocity within each grouping. Positional rms uncertainties

for the spots were estimated both from the position fit errors in each velocity plane and from the scatter in these values across the velocity width of the feature, demonstrating that the uncertainties are generally less than 0.025 arcsec.

The overall spatial pattern of the spots is displayed in Fig. 2. Note that 1 second = 7.12 arcsec at this declination. Many coincidences occur between features of different polarization, and between the transitions. For the purposes of position comparison between features, we treat any offset of up to about one-third of the halfpower beamwidth as a coincidence. Position coincidences of features with different polarization, and/or different transition, result in the 59 spectral features being located in just 28 different spots, as described below.

Ten features of Table 1 have a matching stronger feature in the opposite polarization but at the same position and velocity. For example, 1665 MHz LHC feature q matches stronger RHC feature P. In many similar cases studied in earlier work (e.g. section 4.3 of Fish & Reid 2006), detailed investigation shows such features to be elliptically polarized, sometimes with additional unpolarized emission. Our

Table 1. Polarized features of OH 300.969+1.147; position offsets relative to (J2000) R.A. = $12^h 34^m 53^s.27$, Dec = $-61^\circ 39'39''.63$. Details in section 4.1

Transition and pol.	Feature label	Velocity (km s ⁻¹)	R.A.offset (arcsec)	Dec. offset (arcsec)	Peak flux (Jy beam ⁻¹)	<i>B</i> (mG)	Comment	
<i>1665LHC</i>	a	-34.69	-0.171	-0.045	0.11	-1.1	<i>Z</i> ₁	
	b	-34.97	0.016	-0.004	2.73	-1.3	<i>Z</i> ₂ ; matches <i>Z</i> ₁₃	
	c	-35.71	-0.305	-0.574	1.16	-4.2	<i>Z</i> ₃	
	d	-35.86	-0.119	0.051	0.14	-4.7	<i>Z</i> ₄	
	e	-36.19	-0.169	-0.457	0.16	-4.6	<i>Z</i> ₅	
	f	-36.53	-0.195	-0.653	0.36	-4.5	<i>Z</i> ₆	
	g	-36.78	-0.271	-0.549	0.67	-3.2	<i>Z</i> ₇	
	h	-37.16	-0.283	-0.554	0.25		unpaired	
	i	-37.21	-0.216	-0.664	0.27	-4.0	<i>Z</i> ₈ ; matches <i>Z</i> ₁₅	
	j	-37.92	-0.175	-0.654	2.80	-3.7	<i>Z</i> ₉ ; matches <i>Z</i> ₁₆	
	(k)	-38.15	-0.285	-0.562	0.10		(elliptical with F)	
	(l)	-38.90	-0.168	-0.457	0.20		(elliptical with J)	
	(m)	-39.20	-0.196	-0.652	0.13		(elliptical with K)	
	n	-39.32	0.510	-0.560	0.30	-3.2	<i>Z</i> ₁₀	
	(o)	-40.05	-0.168	-0.652	0.14		(elliptical with M)	
	p	-40.17	0.403	-1.465	1.71	-4.4	elliptical with N; <i>Z</i> ₁₁	
	(q)	-40.28	0.062	-0.305	0.27		(elliptical with P)	
	(r)	-40.86	0.442	-0.529	0.16		(elliptical with R)	
	s	-41.01	0.249	-1.502	0.21	-1.5	<i>Z</i> ₁₂ ; almost matches <i>Z</i> ₁₇	
	(t)	-41.98	0.279	-1.498	0.06		(elliptical with T)	
<i>1665RHC</i>	A	-34.71	-0.125	-0.044	0.10		unpaired	
	B	-35.31	-0.164	-0.043	0.14		<i>Z</i> ₁	
	C	-35.73	0.007	-0.001	1.64		<i>Z</i> ₂	
	D	-37.30	-0.132	0.049	0.27		unpaired	
	E	-37.98	-0.123	0.046	0.15		unpaired	
	F	-38.16	-0.275	-0.558	0.40		elliptical with k; <i>Z</i> ₃	
	G	-38.30	-0.127	0.065	0.09		unpaired	
	H	-38.66	-0.110	0.056	0.13		<i>Z</i> ₄	
	I	-38.65	-0.259	-0.552	0.39		<i>Z</i> ₇	
	J	-38.93	-0.165	-0.452	0.78		elliptical with l; <i>Z</i> ₅	
	K	-39.18	-0.197	-0.653	5.40		elliptical with m; <i>Z</i> ₆	
	L	-39.59	-0.220	-0.671	15.44		<i>Z</i> ₈	
	M	-40.11	-0.177	-0.652	5.52		elliptical with o; <i>Z</i> ₉	
	(N)	-40.16	0.405	-1.461	0.70		(elliptical with p)	
	O	-40.16	-0.508	0.144	0.50		unpaired	
	P	-40.42	0.053	-0.300	0.48		elliptical with q; unpaired	
	Q	-40.40	-0.083	-0.415	0.17		unpaired	
	R	-40.90	0.454	-0.534	0.20		elliptical with r; unpaired	
	S	-41.19	0.508	-0.557	0.43		<i>Z</i> ₁₀	
	T	-41.89	0.292	-1.497	0.40		elliptical with t; <i>Z</i> ₁₂	
U	-42.59	-0.163	-1.378	0.16		unpaired		
V	-42.78	0.439	-1.504	0.57		<i>Z</i> ₁₁		
<i>1667LHC</i>	a	-35.22	0.013	-0.003	2.96	-1.2	<i>Z</i> ₁₃ ; matches <i>Z</i> ₂	
	b	-35.63	-0.104	-0.018	0.18		unpaired	
	c	-36.12	-0.036	0.031	0.08	-1.3	<i>Z</i> ₁₄	
	d	-36.24	-0.275	-0.740	0.12		unpaired	
	e	-37.09	-0.384	-0.602	0.06		unpaired	
	f	-37.73	-0.229	-0.670	0.57	-3.5	<i>Z</i> ₁₅ ; matches <i>Z</i> ₈	
	g	-38.48	-0.176	-0.654	1.38	-3.6	<i>Z</i> ₁₆ ; matches <i>Z</i> ₉	
	(h)	-39.86	-0.184	-0.648	0.10		(elliptical with D)	
	(i)	-40.25	0.052	-0.300	0.28		(elliptical with E)	
	j	-40.54	0.254	-1.491	1.04	-2.0	<i>Z</i> ₁₇ ; almost matches <i>Z</i> ₁₂	
	k	-41.04	0.458	-1.513	0.35		unpaired	
	<i>1667RHC</i>	A	-35.64	0.000	0.000	4.02		<i>Z</i> ₁₃
		B	-36.59	-0.021	0.043	0.13		<i>Z</i> ₁₄
C		-38.97	-0.224	-0.672	4.34		<i>Z</i> ₁₅	
D		-39.74	-0.178	-0.651	0.37		elliptical with h; <i>Z</i> ₁₆	
E		-40.38	0.052	-0.299	0.35		elliptical with i; unpaired	
F		-41.25	0.260	-1.490	0.35		<i>Z</i> ₁₇	

data, without linear polarization analysis, do not distinguish these situations, but for simplicity, we add the comment to q: ‘elliptical with P’, and likewise the comment ‘elliptical with q’ is added to P. The weaker component is not a truly separate feature, and is distinguished in Table 1 by adding parentheses to both its feature label in column 1 and its comment. This particular example is of additional interest because it is not part of a recognisable Zeeman pair, and it is co-located with an unpaired 1667-MHz LHC feature i (similarly possessing a matching stronger feature (E) in RHC polarization).

Spatially coincident features of different circular polarization which have different velocities are expected to be the σ -components of a Zeeman pattern. The σ -components are most generally elliptically polarized, usually with the circular percentage dominating over the linear percentage.

We interpret 34 features as components of 17 Zeeman pairs (12 at the 1665-MHz transition and 5 at 1667 MHz), as noted in the comments column of Table 1; the derived magnetic fields are given in the previous column. The magnetic field values assume Zeeman splitting factors such that, in a 1 mG magnetic field, a spectral line will be split into two components of opposite circular polarization, separated in frequency by an amount equivalent to 0.590 km s^{-1} for the 1665-MHz transition and 0.354 km s^{-1} for the 1667-MHz transition.

Three of the 1667-MHz Zeeman pairs closely match corresponding 1665-MHz Zeeman pairs, as noted in the comments. Zeeman pairs Z12 at 1665 MHz and Z17 at 1667 MHz are co-located, and match in magnetic field, but differ by 0.5 km s^{-1} in their mean velocity. In addition to the 14 different spot positions hosting Zeeman pairs, there are 14 spot positions (one of them with emission at both 1665 and 1667 MHz) which have ‘unpaired’ spectral features i.e. features that are not part of a Zeeman pair.

Further notes on some of the individual spectral features are given below; these include consideration of single dish Parkes spectropolarimetry 2005 November, which obtained full polarimetry at 1665 and 1667 MHz with high spectral resolution but low spatial resolution.

1665 MHz LHC g. Single dish spectra from the Parkes telescope suggest 35 per cent linear polarization of this feature. We note that the Parkes observations were several years later than the LBA observations, and this feature in particular had increased in intensity, but it is useful to explore the possible implications of the Parkes data for interpreting the LBA data. If 35 per cent linear polarization is present in the LBA data, then the maximum possible circular polarization would be 94 per cent, and there would then be an expectation of a LHC component of 0.05 Jy. Since this is close to our detection limit, our non-detection of a LHCP feature is not significant. We conclude that feature g is most likely elliptically polarized, with the RH circular component dominant.

1665 MHz LHC m. Coincidence with feature K is noted as evidence for linear polarization in K. This is supported by the single dish data from Parkes indicating at least 10 per cent linear polarization of this feature.

1665 MHz LHC p. Commented as ‘elliptical with N’. This is supported by single dish spectra from the Parkes telescope showing at least 10 per cent linear polarization at this velocity. The circular polarization is 71 per cent and so if the feature is 100 per cent polarized, then its linear polarization would also be 71 per cent.

1665 MHz RHC L. Single dish spectra from the Parkes telescope suggest 10 per cent linear polarization at this velocity. The maximum possible circular polarization would then be 99.5 per cent, and there would then be an expectation of a LHC component of 0.077 Jy. Although this is not detected, the absence may result from some maser variability in the several years between LBA and Parkes observations. We conclude that, although the RH circular component is dominant, there is likely to be some linear polarization also present, to give net elliptical polarization.

1667 MHz RHC C. Single dish spectra from the Parkes telescope suggest 10 per cent linear polarization at this velocity. The maximum possible circular polarization would then be 99.5 per cent and the expectation of a 20 mJy LHC component. This is below our sensitivity level, so its absence is not significant.

4.2 Velocities, magnetic field, and kinematics

From the median velocity of detected maser features, we can estimate the systemic velocity of OH 300.969+1.147 to be -38 km s^{-1} . The H II region in this direction has a radial velocity of -47 km s^{-1} (Caswell & Haynes 1987b). The ‘tangent point’ velocity, the most negative ‘allowed’ velocity in this direction for commonly used Galactic rotation models, is -40 km s^{-1} . We conclude that the maser and H II region are close to the tangent point, and thus at a uniquely defined distance of 4.3 kpc (if the Galactic Centre is assumed to be at 8.5 kpc from the Sun; or 5.1 kpc distant if the Galactic Centre were at 10 kpc, the value assumed in older studies).

Considering the Zeeman pairs in more detail, we note that, throughout the whole site, the estimates of magnetic field for all 17 Zeeman pairs are notably in the same sense (towards the observer, as denoted by a negative field) and range from -1.1 to -4.7 mG , with a median value of -3.5 mG .

Further information on the magnetic field is provided by excited-state OH 6035- and 6030-MHz masers. A position measurement for strong 6035-MHz emission at -37.5 km s^{-1} (Caswell 1997) yields a position RA $12^{\text{h}} 34^{\text{m}} 53.27^{\text{s}}$, Dec. $-61^{\circ} 39' 39.9''$. The spectra in Fig. 1 of Caswell (2003) show that this 6035-MHz reference feature is a Zeeman pair arising in a magnetic field of -5.0 mG , and is accompanied by an OH 6030-MHz pair indicative of a similar field. Two other weak 6035-MHz Zeeman pairs corroborate this field strength. The 6035-MHz position is shown on Fig. 2 as a dotted square; the uncertainty in the position is larger than the square, with contributions from the absolute position registration for both species, but the location lies, encouragingly, amongst a high concentration of 1665- and 1667-MHz maser spots of which several reveal similar magnetic fields. Indeed, it may be closely associated with the OH 1665-MHz Zeeman pair Z5 which has essentially the same magnetic field (-4.6

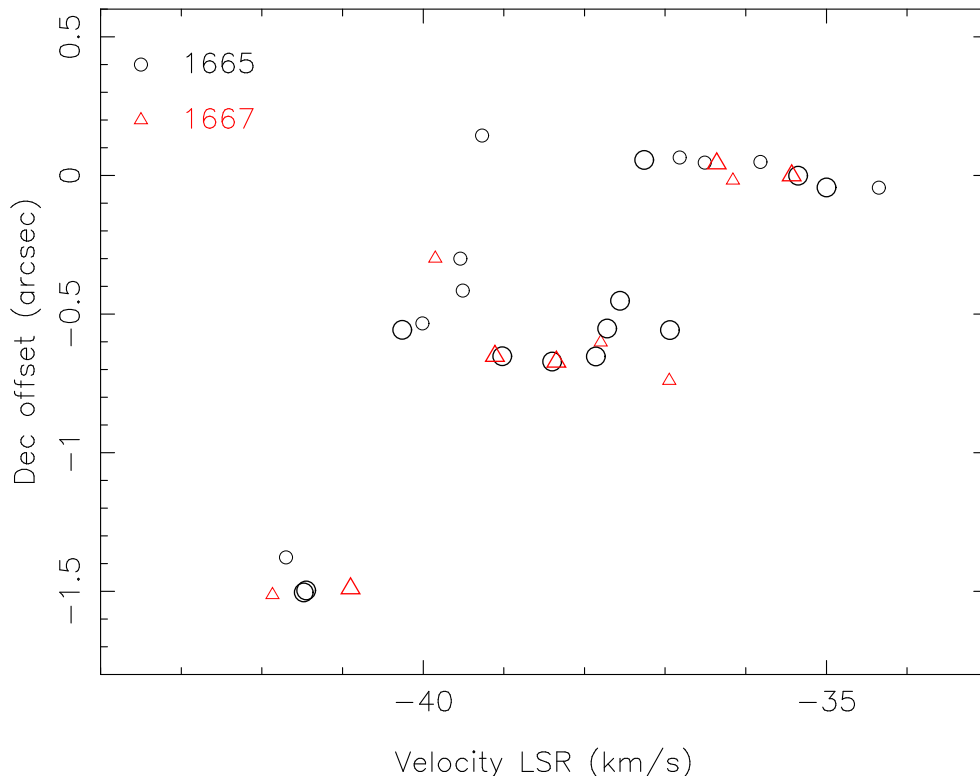


Figure 3. Declination of each maser spot is plotted against ‘demagnetized’ velocity. Each large symbol corresponds to a Zeeman pair with its mean velocity plotted, and each small symbol is an unpaired single feature with velocity adjusted as described in Section 4.2

mG), same mean velocity, and is coincident (the offset of 0.23 arcsec is smaller than the registration uncertainty).

The 6-GHz ATCA observations (Caswell 1997) also reveal a weak methanol 6668-MHz maser close to the OH 6035-MHz maser, and superposed on a uCH II region with flux density 164 mJy at 6 GHz. Lower resolution maps of the region at 5 GHz reveal a much higher flux density of 3.1 Jy extending over an estimated size of 1 arcmin (Caswell & Haynes 1987b), so the region is clearly quite complex, with additional emission on a much more diffuse scale than 1 arcsec. In the absence of full mapping of the uCH II region, its boundary is sketched as a large dotted circle on Fig. 2 circumscribing the maser spots and consistent with its absolute position measurement.

We now explore the kinematics, and whether the velocity field, as derived from the combination of the spatial distribution of the maser spots and their radial velocities, might reveal a pattern indicative of rotation or expansion.

However, we ought first to correct for the fact that velocity values at 1665 and 1667 MHz are not purely kinematic and have been significantly affected by the magnetic field. In order to obtain a corrected velocity estimate at each position, we first use the mean velocity value for each of the 17 Zeeman pairs. The corrections relative to individual spot velocities range from 0.18 km s^{-1} for the lowest-field 1667-MHz feature to nearly 1.5 km s^{-1} for the highest-field 1665-MHz feature. For the other (15) unpaired features, we must first decide whether they are more likely to be π -components or lone surviving σ -components from Zeeman patterns. We note that none of them has location and velocity compatible with being the π -component of any of our recognized

Zeeman pairs, and regard them as most likely lone surviving σ -components. We ‘correct’ their velocities by assuming that they originated in the same field as their nearest Zeeman pair companion. All ‘corrected’ velocities were then inspected over the whole map and the only suggestive pattern was an apparent gradient of velocity with declination. A plot of velocity against declination was then made, and is shown in Fig. 3. Large symbols are used for the Zeeman patterns since they represent the information from 2 spots rather than 1, and have more reliable corrections. Fig. 3 reveals a tendency for more negative velocities to be at the south of the distribution, with gradient of approximately 4 km s^{-1} over 1 arcsec. Naively we could regard this as indicating rotation about an east-west axis.

4.3 Properties of the site as a whole

With regard to other OH transitions, we note the detection of a loosely associated 1720-MHz maser (Caswell 2004) at (J2000) RA $12^{\text{h}}34^{\text{m}}53.63^{\text{s}}$, Dec. $-61^{\circ}39'40.0''$) with uncertainty $0.4''$. It lies outside the region shown in Fig. 2, with an offset to larger RA by 0.36s ($= 2.6''$) and south by $0.4''$ from the reference location used in this study (for Table 1 and Fig. 2). The 1720-MHz maser displays a clear Zeeman pattern indicative of a magnetic field of -5 mG , with mean velocity -42.5 km s^{-1} . It lies in a broad absorption dip extending from -39 to -47 km s^{-1} , presumably indicative of a dense, more extensive, host molecular cloud. The spatial offset of the 1720-MHz maser from our current object of study seems large enough to rule out a common source of excitation, but it clearly lies in the same region of massive star

formation. This is corroborated by its radial velocity and its magnetic field value, both of which are in the same range as our 1665 and 1667-MHz measurements.

There has been no detection of OH at the 1612-MHz transition (Caswell 1999).

In addition to the presence of the previously mentioned methanol maser at the 6668-MHz transition, there is a methanol maser at the 12-GHz transition with a weak peak at the same velocity (Caswell et al. 1995).

Water maser emission peaking above 40 Jy and covering the velocity range -43 to -86 km s $^{-1}$ (Caswell et al. 1989) was reported at approximately this position but is now found (Caswell, ATCA unpublished data) to be offset 18 arcsec, and thus not closely related.

The general location of the star formation complex is at a Galactic latitude of more than 1° where, with 301.109+0.969 (Caswell & Haynes 1987b), it is one of only two prominent star forming regions in this portion of sky. Their separation of 0.246° corresponds to 18 pc. This comparative isolation will allow detailed future studies to be undertaken unaffected by other nearby companion star clusters, an isolation which can be especially valuable when investigating the more common molecular species that are able to trace the properties of a massive-star-forming environment.

Summarizing the properties, we conclude that the region, although young enough to host masers of OH and methanol, is mature enough to have a prominent uCH II region. The relative weakness of methanol, plus the absence of an intimately associated water maser, are also common properties of these more mature regions (Caswell 1997). The complex as a whole does, however, also host a water maser, a 1720-MHz OH maser, and a more extensive OH cloud (responsible for a prominent feature of 1720 MHz absorption against the extended H II region). The consistency of magnetic field direction within the source (and even at the location of 1720-MHz emission) also reinforces its status as a stable region which is approaching the end of the short evolutionary period that can support maser emission, according to current ideas (Caswell & Reynolds 2001).

4.4 Comparison of OH 300.969+1.147 with other maser sites

The most recent major addition to high resolution mapping of OH masers is from a study of 18 targets with the VLBA by Fish, Reid, Argon & Zheng (2005), discussed in detail by Fish & Reid (2006). Very few targets conform precisely to the canonical picture, in which maser spots appear projected onto a simple uCH II region, with magnetic field estimates all of the same sign, and some kinematic order discernible.

Most of the VLBA targets lie in the Galactic first quadrant, longitude 0 to 90° , and the only one, 351.775-0.536 that lies in the fourth quadrant (longitude 270 to 360°) is not covered over its full velocity range.

The present observations add another example from the largely untapped resource of southern fourth quadrant masers and establishes another simple morphology against which we can compare the more pathological ones.

In a previous study (Caswell & Reynolds 2001), we compared the properties of OH 323.459-0.079 with those of the archetypical W3(OH), and concluded that it was similar, but

slightly larger in linear extent and weaker, and thus perhaps slightly older. The present target also appears larger (largest separation of maser spots is 36 mpc), weaker, and it has relatively weaker methanol maser emission and no water maser. All of these slight differences conform to expectations for a slightly more evolved maser site.

Maser sites show a weak tendency to display a magnetic field direction in the sense of Galactic rotation, and indeed the present target conforms to this, with a field towards us in the Galactic fourth quadrant. Some counter-examples such as OH 34.257+0.154 occur in crowded and apparently disturbed regions of the Galactic plane which may be relevant. However, OH 323.459-0.079 shows a magnetic field counter to Galactic rotation, and yet lies in an apparently undisturbed region. Indeed, it lies at similar distance, and in the same (Crux-Scutum) spiral arm as OH 300.969+0.147, with its main point of difference being its location at the inner edge of the arm rather than the outer edge. Another notable counter-example is 285.263-0.050 which appears to lie close to the centre of the Carina arm. Thus at present, there is no evidence that the counter-examples are merely exceptions to a general rule because of their exceptional circumstances. Rather, the relation appears somewhat weak in its significance.

5 CONCLUSION

In the common picture of OH masers in massive young stellar objects, a cluster of maser spots is projected against an uCH II region of diameter about 30 mpc, with the pattern of maser spots revealing a magnetic field of a few mG, and a small velocity range of less than 10 km s $^{-1}$, with velocity field perhaps indicative of rotation. The detailed study of W3(OH) has defined this archetype, but finding additional real examples conforming to this pattern has proved difficult. The present study establishes OH 300.969+1.147 as a new example conforming to this simple pattern, and we regard it as a mature region nearing the end of the brief evolutionary period that can support maser emission. Examples of these canonical maser sites are important for comparison with other diverse sites that have no discernible uCH II region (perhaps younger), or with maser spots scattered over a larger area (perhaps multiple sources), magnetic fields more complex, and velocity patterns suggestive of outflows.

ACKNOWLEDGMENTS

We thank the ATNF staff who make the intricate operation of the LBA successful, and fellow astronomers who participated in the observing session. BHK thanks ATNF for hospitality and funding as a distinguished visitor during some of the period when this work was performed.

REFERENCES

- Caswell J.L., 1997, MNRAS, 289, 203
- Caswell J.L., 1998, MNRAS, 297, 215
- Caswell J.L., 1999, MNRAS, 308, 683
- Caswell J.L., 2003, MNRAS, 341, 551
- Caswell J.L., 2004, MNRAS, 349, 99

- Caswell J.L., Haynes R.F., 1987a, *Aust.J.Phys.*, 40, 215
Caswell J.L., Haynes R.F., 1987b, *A&A*, 171, 261
Caswell J.L., Reynolds J.E., 2001, *MNRAS*, 325, 1346
Caswell J.L., Batchelor R.A., Forster J.R., Wellington K.J., 1989,
Aust.J.Phys., 42, 331
Caswell J.L., Vaile R.A., Ellingsen S.P., Norris R.P., 1995, *MN-
RAS*, 274, 1126
Fish V.L., Reid M.J., Argon A.L., Zheng X,W., 2005 *ApJS*, 160,
220
Fish V.L., Reid M.J., 2006, *ApJS*, 164, 99
Robinson B.J., Caswell J.L., Goss W.M., 1974, *Aust.J.Phys.*, 27,
575

This paper has been typeset from a $\text{T}_{\text{E}}\text{X}/\text{L}^{\text{A}}\text{T}_{\text{E}}\text{X}$ file prepared by the author.